APL Photonics

Near ultraviolet photonic integrated lasers based on silicon nitride

Cite as: APL Photonics **7**, 046108 (2022); https://doi.org/10.1063/5.0081660
Submitted: 09 December 2021 • Accepted: 14 March 2022 • Published Online: 25 April 2022

Anat Siddharth, Thomas Wunderer, Grigory Lihachev, et al.

Near ultraviolet photonic integrated lasers based on silicon nitride

Cite as: APL Photon. 7, 046108 (2022); doi: 10.1063/5.0081660
Submitted: 9 December 2021 • Accepted: 14 March 2022 •
Published Online: 25 April 2022

Anat Siddharth,[1] Thomas Wunderer,[2] Grigory Lihachev,[1] Andrey S. Voloshin,[1] Camille Haller,[3] Rui Ning Wang,[1] Mark Teepe,[2] Zhihong Yang,[2] Junqiu Liu,[1] Johann Riemensberger,[1,a)] Nicolas Grandjean,[3] Noble Johnson,[2] and Tobias J. Kippenberg[1,a)]

AFFILIATIONS

[1] Laboratory of Photonics and Quantum Measurements, Swiss Federal Institute of Technology Lausanne (EPFL), CH-1015 Lausanne, Switzerland

[2] Palo Alto Research Center, Palo Alto, California 94304, USA

[3] Laboratory of Advanced Semiconductors for Photonics and Electronics, Swiss Federal Institute of Technology Lausanne (EPFL), CH-1015 Lausanne, Switzerland

[a)] **Authors to whom correspondence should be addressed:** johann.riemensberger@epfl.ch and tobias.kippenberg@epfl.ch

ABSTRACT

Low phase noise lasers based on the combination of III–V semiconductors and silicon photonics are well established in the near-infrared spectral regime. Recent advances in the development of low-loss silicon nitride-based photonic integrated resonators have allowed them to outperform bulk external diode and fiber lasers in both phase noise and frequency agility in the 1550 nm-telecommunication window. Here, we demonstrate for the first time a hybrid integrated laser composed of a gallium nitride-based laser diode and a silicon nitride photonic chip-based microresonator operating at record low wavelengths as low as 410 nm in the near-ultraviolet wavelength region suitable for addressing atomic transitions of atoms and ions used in atomic clocks, quantum computing, or for underwater LiDAR. By self-injection locking of the Fabry–Pérot diode laser to a high-Q (0.4×10^6) photonic integrated microresonator, we reduce the optical phase noise at 461 nm by a factor greater than 100×, limited by the device quality factor and back-reflection.

INTRODUCTION

Photonic integrated lasers that operate in the visible to ultraviolet (UV) spectral regime featuring narrow emission linewidth and low phase noise are required for the miniaturization of photonic systems. Applications for such systems range from quantum metrology and sensing[1] based on laser-cooled neutral atoms and ions[2] to precision atomic clocks,[3] underwater laser range-finding,[4] interferometric biophotonics,[5] and visible spectroscopy.[6,7] The wide bandgap group III-nitride semiconductor material family is ideally suited as an active material platform for next-generation integrated photonics covering operation wavelengths in the UV and visible spectral regime. High power III-N laser sources [i.e., gallium nitride (GaN) and its alloys] are commercially available today and can be found in various products such as Blu-ray players, solid-state lighting devices, or modern car headlamps. However, for neutral atom and ion-based quantum information science and metrology applications, conventional III-N laser diodes cannot meet the requirements in terms of emission linewidth (i.e., phase noise) and longitudinal mode stability (i.e., drift) during operation. Instead, only external cavity diode lasers using bulk precision optics and gratings, which are frequency tuned via physical adjustment, have achieved a suitable performance, exhibiting kHz linewidth.[8] Yet, the bulk nature of these laser systems along with their weight restricts applications, in particular space-based applications. More compact blue lasers have been demonstrated based on crystalline resonators, yet these are not wafer-scale compatible.[9] As a result, the development of single-frequency III-N lasers has regained interest. These include distributed feedback laser configurations for single-frequency operation.[10–14] In contrast, silicon photonics-based lasers using heterogeneous[15] and hybrid integration[16] have enabled scalable, narrow linewidth,[17] and tunable lasers[18] that outperform bulk

external diode and fiber lasers and are already employed at a commercial level in data center interconnects, typically operating in the 1550 nm-telecommunication window.[19] Yet, silicon's bandgap limits its access to a shorter wavelength. Silicon nitride (Si_3N_4) is a good material to realize low loss integrated photonic circuits in the visible and ultraviolet wavelength spectral region due to a wide bandgap of 4.9 eV, a high refractive index of 2.09 at 410 nm, CMOS-compatible fabrication, and established commercial foundry processes. Moreover, major advances in nano-fabrication methods have enabled ultra-low propagation loss waveguides, reaching 1 dB/m.[20] Demonstrations using the Si_3N_4 platform in the visible regime so far include blue laser-based beam-forming,[21] biophotonic probes,[22] modulators,[23] and visible photonic integrated lasers.[24] Laser cooling of atoms and ions (e.g., Ca^+ at 397 nm, Yb at 399 nm, Sr^+ at 420 nm, and Sr at 461 nm) requires a laser wavelength close to 400 nm [cf. Fig. 1(f)] with typical $\mathcal{O}$(mW) power levels. Integrating compact III-N laser gain elements with high-performance Si_3N_4-based photonic circuits for single-frequency laser operation with narrow linewidth at wavelengths close to 400 nm has not yet been attained, and the prospect for tunability and stable operation has not been explored in great detail. Here, the hybrid integration of an AlGaInN laser gain element coupled to a Si_3N_4 photonic integrated circuit (PIC) platform featuring a laser intrinsic linewidth of ~1.15 MHz is demonstrated with more than 20 dB frequency noise reduction via laser self-injection locking. Such narrow linewidth laser sources, which via integration of AlN or PZT piezoelectric actuators can also be made frequency-agile, i.e., enable mode-hop free scanning over $\mathcal{O}$(10 GHz) with the actuation bandwidth of $\mathcal{O}$(10 GHz) as

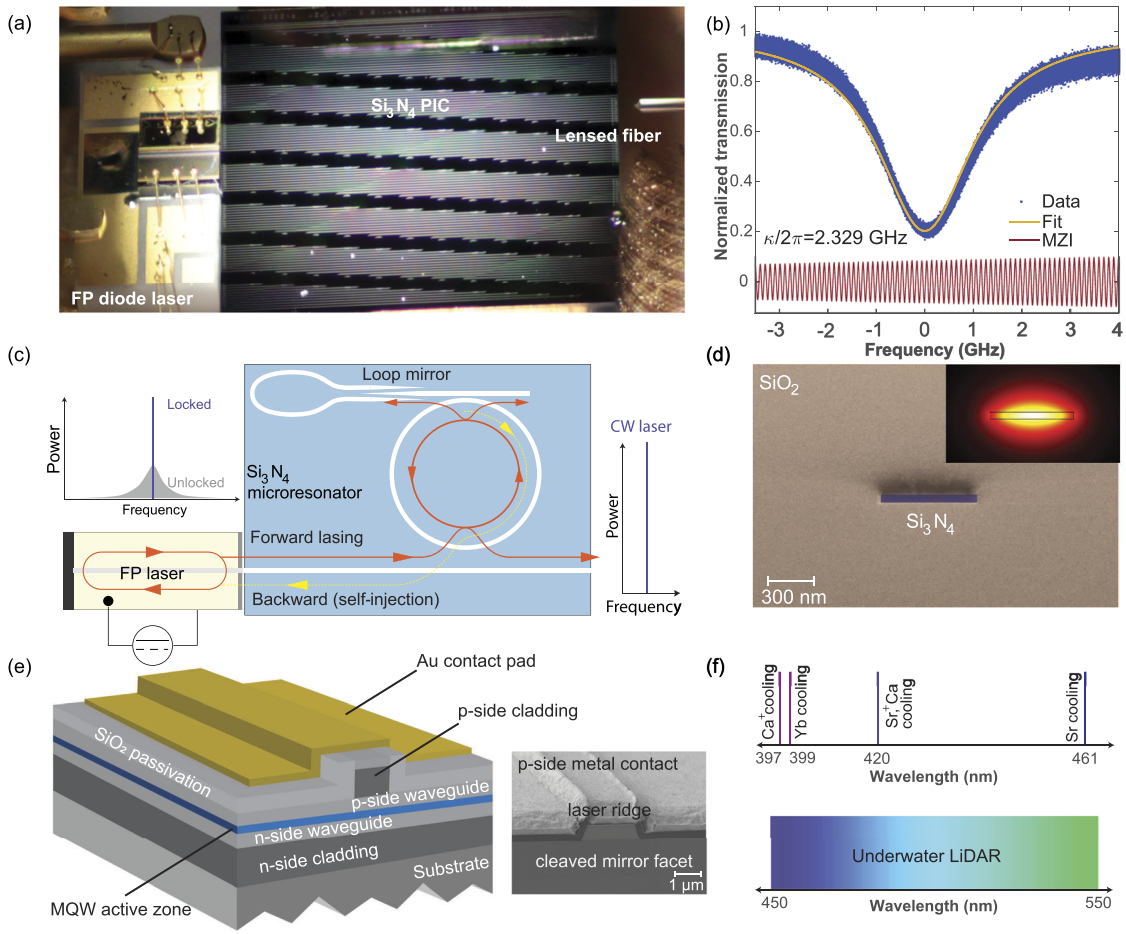

FIG. 1. Schematic of the hybrid integrated laser system. (a) Photo of the experimental setup showing the Fabry–Pérot laser diode butt-coupled to the Si_3N_4 photonic chip and the output radiation is collected by a lensed fiber. (b) Si_3N_4 resonance measured using a tunable laser at 461 nm calibrated by a fiber-based Mach–Zehnder interferometer with a free spectral range of 100.12 MHz. The measured loaded linewidth $\kappa/2\pi \approx 2.33$ GHz, corresponding to the loaded quality factor of 0.28×10^6. This microresonator did not have a drop-port. (c) Principle of laser linewidth narrowing via laser self-injection locking. (d) False-colored scanning electron microscope (SEM) image of the sample cross-section, showing a 50 nm thick Si_3N_4 buried in the SiO_2 cladding of total thickness 6 μm. The inset shows a finite element method (FEM) simulation of the spatial distribution of the TE-mode electric-field amplitude at wavelength 461 nm. (e) Schematic showing the laser diode structure with near-UV (410 nm) emission with the SEM image of the sample cross-section showing the laser ridge. (f) Different applications for III-N integrated lasers presented at wavelength schematics, including underwater LiDAR and ion transitions used for cooling.

recently demonstrated,[18] are ideal candidates for photonic integrated lasers for manipulating trapped-ion/atomic quantum systems or underwater coherent laser ranging.

RESULTS

III-N semiconductor-based hybrid self-injection locked lasers using Si_3N_4 integrated photonics

Figures 1(a) and 1(b) depict the experimental setup with a GaN-based Fabry–Pérot laser diode chip directly butt-coupled to a Si_3N_4 photonic chip. Custom AlGaInN near-UV laser diodes were fabricated on low-defect density native GaN substrates using Metal-Organic Vapor Phase Epitaxy (MOVPE). The epitaxial growth process was optimized toward high gain and low absorption losses within the laser heterostructure, balancing the optical and electronic performance of the device. The active zone of the laser diode consists of multiple InGaN quantum wells that are electrically pumped in a pn-junction architecture. The design was tailored for laser emission near 410 nm and is depicted in Fig. 1(e). In this edge-type emitter configuration, transversal mode confinement is realized through the heterostructure layer stack where the active Multi-Quantum Well (MQW) zone is embedded in the (Al)Ga(In)N waveguide and cladding layers featuring different Al-compositions. Lateral mode confinement is achieved via dry etching a narrow ridge into the p-side of the heterostructure and the creation of optical gain in the QWs right below the etched ridge. Lateral current confinement and the creation of localized gain are accomplished by ensuring electrical current injection exclusively through an opening in the electrical passivation layer on top of the laser ridge [cf. Fig. 1(e)]. The laser ridge had a width of nominally 1.5 μm and was etched to an optimized depth for laser operation of only one lateral mode. Laser mirror facets were realized via cleaving along the crystallographic m-plane of the III-N crystal. The laser resonator cavities were about 1 mm long. Optical facet coatings were applied to both the front and the rear facet for optimized laser characteristics. For full continuous wave (CW) operation, individual laser dies (LD) were mounted epi-side up onto thermal heat spreader sub-mounts and individually wire-bonded for both the n- and p-side. The LD-heat spreader sub-mount ensemble was then mounted into a standard TO-5 can. Special care was taken to allow for excellent laser facet exposure for optimal butt-coupling of the LD to the Si_3N_4 chip. The laser diode showed a characteristic laser threshold of about 70 mA and can produce more than 100 mW of optical output power at a wavelength of 410 nm (cf. Fig. 1 of the supplementary material). The laser is mounted on a thermo-electric cooler for stabilizing its temperature and is operated at 21 °C.

In addition, in this work, we also investigate longer wavelength lasers, notably blue and green laser diodes (LDs), which were provided by Exalos AG.[25] The emission wavelength of the commercially available blue LD is between 457 and 464 nm with a threshold current around 18 mA. The green LD has an emission wavelength between 517 and 523 nm with a threshold current of around 38 mA.

The Si_3N_4 waveguides and microresonators are fabricated using a subtractive process[26] and have a uniform height and width of 50 and 600 nm, respectively. Stoichiometric Si_3N_4 thin films are grown with low-pressure chemical vapor deposition (LPCVD) and etched in fluorine chemistry. The waveguides and microresonators are defined by deep-ultraviolet stepper (248 nm) lithography. The cross-section of the microresonators of the Si_3N_4 waveguide is depicted in Fig. 1(d). The waveguides are fully buried in the SiO_2 cladding of 7 μm thickness. The bottom cladding is made of a thermal oxide of 4 μm thickness, whereas the top cladding is composed of 1 μm TEOS and 2 μm low-temperature oxide (LTO). The entire device sits on a 230 μm thick Si substrate. The radius of the microresonator is 200 μm, corresponding to the free spectral range of ~107.08 GHz. The thin Si_3N_4 supports the fundamental transverse electric (TE) mode at violet and blue wavelengths as shown in the inset with ~14.5% of the E-field confined in the Si_3N_4 core as shown in the inset of Fig. 1(d). Development of a low loss photonic platform in the blue and near-ultraviolet spectral regime is challenging due to scattering and absorption losses.[27] Rayleigh scattering scales with λ^{-4}, and material loss also increases as wavelengths approach the materials' bandgap. Figure 1(b) presents a cavity linewidth measurement of the Si_3N_4 microresonator without a drop-port, carried out at 461 nm (see Fig. 2 of the supplementary material for resonance characterization at a higher wavelength), which reveals a loaded cavity linewidth $\kappa/2\pi$ = 2.33 GHz and an intrinsic linewidth $\kappa_0/2\pi$ = 1.69 GHz, corresponding to an intrinsic quality factor of ~0.4×10^6 (corresponding to a propagation loss of ~3 dB/cm). The quality factor can be enhanced by designing waveguides with higher aspect ratios and making a thinner Si_3N_4 core.[28] Such a design takes advantage of the lower material loss of the silica cladding and reduces the mode overlap with the sidewalls, which minimizes sidewall scattering, which is the primary contributor to loss in high-index-contrast planar waveguides. The Si_3N_4 waveguide has a horn-tapered waveguide at the input facet to enhance butt-coupling efficiency with the laser diode and an inverse tapered waveguide at the output facet to couple light to the lensed fiber. The butt-coupling scheme gives an overall insertion loss of ~7.5 dB (diode-PIC-lensed fiber), which we measure by comparing the free-space output power of the laser with the fiber-coupled power in the free-running laser regime. The insertion loss can be further reduced by using bi-layer silicon nitride edge couplers[29] that enhance fiber-to-chip light coupling in the visible wavelength regime.

Figure 1(c) illustrates the laser self-injection locking principle. The key parameters that influence self-injection locking are the quality factor of the microresonator, Rayleigh backscattering, and the optical feedback phase (optical phase of backscattered light). We tune the current of the laser diode and thus sweep the relative frequency between the laser and the resonator modes to attain self-injection locking. When the frequency of the light emitted from the laser diode is close to a high-Q resonance of the Si_3N_4 microresonator, laser self-injection locking takes place (see Fig. 3 of the supplementary material for the cavity transmission trace at different operating points). The process occurs due to the coupling of counter-propagating microresonator modes induced by Rayleigh scattering[30,31] and the light reflected by the loop-mirror present at the drop-port of the microresonator as shown in Fig. 2(c). Figure 2(d) shows the optical transmission and reflection spectra of a critically coupled device having such a loop mirror as a reflector at its drop-port.[32] This configuration provides a frequency-selective narrowband optical feedback to the laser, leading to a single-frequency operation and a reduction in the laser's frequency noise within the locking range.[33] The self-injection locked laser will not hop within the locking range. Still, it will hop if we use a

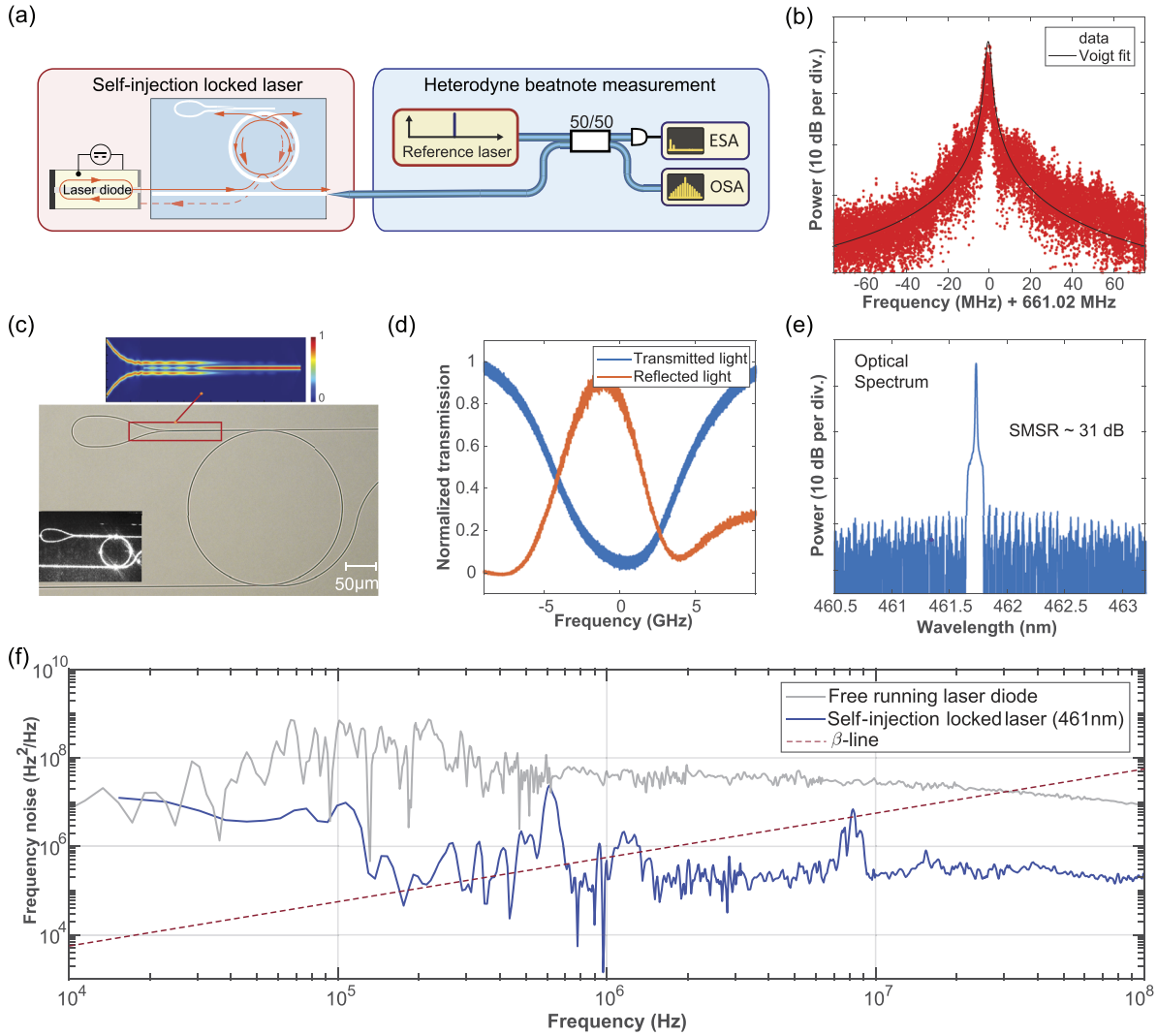

FIG. 2. III-N hybrid integrated laser performance characterization at 461 nm. (a) Experimental scheme of laser frequency noise measurement using the heterodyne beat with the reference laser (Toptica DLC DL pro HP) at 461 nm. (b) The heterodyne beat signal between the injection-locked laser and the reference laser. The measured beat signal is fitted with the Voigt profile with Lorentzian FWHM ~1.156 MHz and Gaussian FWHM ~1.618 MHz. (c) Microscopic image of the 107.08 GHz microresonator with the loop-mirror as the reflector at the drop-port. The input to the loop-mirror is an adiabatically tapered splitter comprising three tapered waveguides as shown in the inset, depicting FDTD simulation of the adiabatically tapered splitter. Another inset shows a photograph of the device with 461 nm wavelength light coupled to it. (d) Optical transmission and reflection spectra of the device shown in (c), measured using the reference laser. (e) Optical spectrum of the self-injection locked Fabry–Pérot laser, showing emission at 461.5 nm with 31 dB side-mode suppression ratio (SMSR). (f) Single sideband frequency noise PSD of the hybrid integrated laser upon self-injection locking to the microresonator with FSR 107.08 GHz. The gray line shows the frequency noise of a free-running Fabry–Pérot laser diode (cf. Fig. 5 of the supplementary material). The β-line is shown as a reference (dashed line).

different locking state that depends on the applied current to the laser diode, its temperature, and the feedback phase from the microresonator (see Fig. 4 of the supplementary material for the locking range of the self-injection locked laser).

Laser frequency noise measurements

Figure 2(a) illustrates the experimental scheme to measure the frequency noise of the laser. The laser frequency noise is measured by performing heterodyne beat-note spectroscopy with a tunable external cavity diode laser (Toptica DLC DL pro HP) with a central wavelength at 461 nm as the reference. The electrical output of the photodiode is fed to a spectrum analyzer (Rhode and Schwarz FSW43). Figure 2(b) shows the heterodyne beat-note of the self-injection locked laser with the reference laser. The spectrum is fitted with the Voigt profile, which provides information about the Lorentzian and Gaussian contribution to the frequency noise of the

laser. The Lorentzian part is linked to the white noise and defines the intrinsic linewidth, whereas the Gaussian part corresponds to the 1/f (flicker) and technical noise of the laser.[34] From fitting, we extract a Lorentzian linewidth of 1.156 MHz and a Gaussian linewidth of 1.618 MHz. The frequency noise measurement is limited by the frequency noise of the reference laser, and its linewidth is 500 kHz according to its specifications.

Figure 2(f) shows the frequency noise spectra of the free-running Fabry–Perot laser and the self-injection locked laser. The frequency noise of the laser is determined via Welch's method[35] from a time sampling trace of the in-phase and quadrature components of the beat-note. The single-sided phase noise power spectral density (PSD) $S_\phi(f)$ was converted to frequency noise $S_\nu(f)$ according to $S_\nu(f) = f^2 \cdot S_\phi(f)$. The self-injection locked laser optical spectrum is shown in Fig. 2(e), indicating the laser emission wavelength at 461.5 nm with a side-mode suppression ratio (SMSR) of 31 dB. We also use the beta-line to quantify the linewidth of the self-injection locked laser by integrating the PSD from the intersection of the frequency noise curve with the beta-line $S_\nu(f) = 8\ln(2)f/\pi^2$ down to the integration time of the measurement. The integrated frequency noise A is used to evaluate the full-width half-maximum measure of the linewidth using[36] FWHM = $\sqrt{8 \cdot \ln(2) \cdot A}$. We evaluate the FWHM as 3.15 MHz at 10 μs integration time and 3.55 MHz at 0.1 ms integration time in agreement with the Voigt fit. The laser self-injection locking suppresses the frequency noise by at least 20 dB across all frequency offsets.

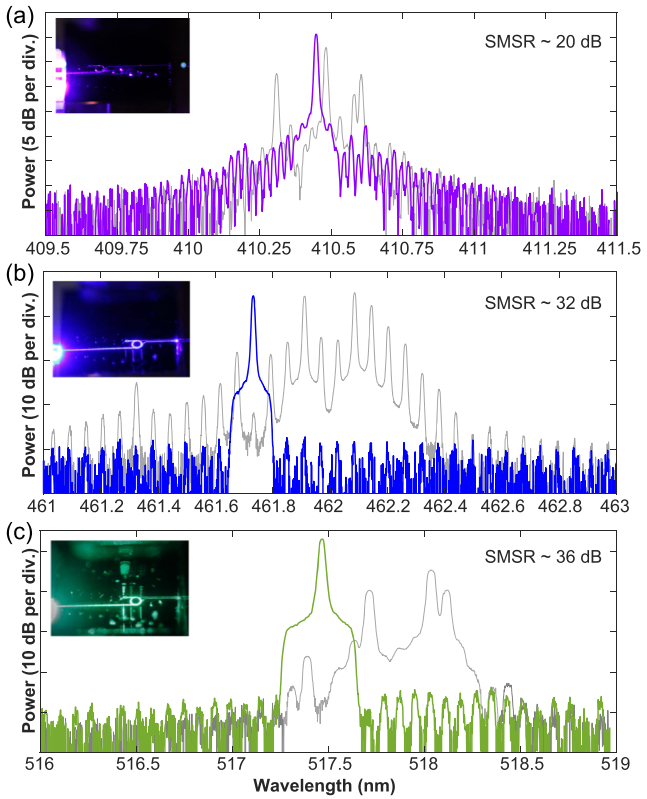

FIG. 3. Single-frequency lasing in near-ultraviolet and visible range. Optical spectra of self-injection locked laser states (single frequency) and multi-frequency free-running laser states (gray lines) at different wavelengths [(a) near-ultraviolet, (b) blue, and (c) green] using the same Si_3N_4 photonic chip (D97F4C9). The insets show photos of the self-injection-locked lasers at respective wavelengths.

Single-frequency lasing in near-ultraviolet and visible regime

Next, we demonstrate the self-injection locked laser in the near-ultraviolet (410 nm) as well as in the green wavelength range using the same Si_3N_4 photonic chip as shown in Fig. 3. Coupling the custom AlGaInN near-UV laser diode with emission at 410 nm (nominal output power of 3.5 mW), we achieve laser self-injection locking at a diode current of 110 mA and voltage of 11 V with a fiber-coupled output power of 0.185 mW. As shown in Fig. 3, we achieve single-frequency lasing at 410.3 nm with a side-mode suppression ratio greater than 20 dB. This constitutes the shortest wavelength hybrid integrated laser-based on Si_3N_4. The inset shows a photograph of the experimental setup where the laser diode is butt-coupled to the Si_3N_4 photonic chip. We clearly observe the scattering of near-ultraviolet light around the circumference of the Si_3N_4 microresonator, which is indicative of the light traveling inside the cavity. We also show operation in the visible regime. We attained single-frequency lasing at blue (461.8 nm) and green wavelengths (518.6 nm) via self-injection locking. The fiber-coupled output powers were 1.1 and 1.9 mW with side-mode suppression ratios of 32 and 36 dB, respectively. The blue laser diode was operated at 52 mA and 4.6 V, whereas the green laser diode was operated at 83 mA and 6.5 V. Optical spectrum analyzer (Yokogawa AQ6373B) wavelength resolution was set to 0.01 nm.

CONCLUSION

In conclusion, we have demonstrated a hybrid photonic integrated laser operating at near-ultraviolet wavelengths as low as 410 nm for the first time. The custom AlGaInN-based laser gain elements were butt-coupled to a Si_3N_4 integrated photonic microresonator with high-Q for optical feedback and mode selection. For the photonic chip, we use Si_3N_4 photonic integrated circuits with a thickness of 50 nm and a uniform width of 600 nm delivering an intrinsic quality factor of 0.4×10^6 at a wavelength of 461.8 nm. The high-quality factor of our platform ensures single longitudinal mode lasing at green to near-ultraviolet wavelengths with linewidths as low as ~1.15 MHz at 461.8 nm that are traditionally only achieved in bulk external cavity diode lasers. Further improvements of the device quality factor are possible by decreasing the Si_3N_4 waveguide core thickness, improving the waveguide roughness by using the photonic Damascene reflow process,[20,37] and by improving the top oxide cladding[38] as well as by weakening confinement, which, however, comes at the cost of increasing the minimum bending ring radius and device footprint. We believe that by optimizing both the coupling between the laser-to-chip and chip-to-fiber and modest improvements in device quality factor, we can achieve multi-mW output powers and sub-100 kHz optical linewidths in the near-ultraviolet region, which would make our systems promising

candidates for compact laser implementations for, e.g., Sr^+ and Ca^+ atomic clocks.

SUPPLEMENTARY MATERIAL

Figures showing the power levels of the custom AlGaIn laser, resonance characterization of the Si_3N_4 device at higher wavelength, transmission trace of different self-injection locked states, locking range and stability of the self-injection locked laser, and spectrum of the free-running Fabry–Pérot laser can be found in the supplementary material.

ACKNOWLEDGMENTS

The authors want to express their gratitude to Christopher Chua and Max Batres at PARC for their contributions to laser fabrication and characterization. They would also like to thank Arslan S. Raja, Jijun He, and Viacheslav Snigirev for their assistance in the experiments.

This work was sponsored by the Army Research Laboratory under Agreement No. W911NF-19-2-0345, by the Army Research Office under Cooperative Agreement No. W911NF-20-2-0214, and by the Air Force Office of Scientific Research under Award No. FA9550-21-1-0063. This work was further supported by the Swiss National Science Foundation under Grant Agreement No. 176563 (BRIDGE). A.S. acknowledges support from the European Space Technology Centre with ESA Contract No. 4000135357/21/NL/GLC/my, and J.R. acknowledges support from the Swiss National Science Foundation under Grant No. 201923 (Ambizione). A.V. is supported by the EU H2020 research and innovation program under the Marie Sklodowska-Curie grant agreement No 101033663 (RaMSoM). The U.S. Government is authorized to reproduce and distribute reprints for government purposes notwithstanding any copyright notation thereon.

The views and conclusions contained herein are those of the authors and should not be interpreted as necessarily representing the official policies or endorsements, either expressed or implied, of the Army Research Laboratory (ARL) or the U.S. Government.

AUTHOR DECLARATIONS

Conflict of Interest

The authors have no conflicts to disclose.

DATA AVAILABILITY

The code and data used to produce the plots within this work will be released on the repository Zenodo upon publication of this preprint.

REFERENCES

[1] G. Moody, V. J. Sorger, P. W. Juodawlkis, W. Loh, C. Sorace-Agaskar, M. Davanco, L. Chang, J. E. Bowers, N. Quack, C. Galland *et al.*, "Roadmap on integrated quantum photonics," J. Phys. Photonics **4**, 012501 (2022).

[2] R. J. Niffenegger, J. Stuart, C. Sorace-Agaskar, D. Kharas, S. Bramhavar, C. D. Bruzewicz, W. Loh, R. T. Maxson, R. McConnell, D. Reens *et al.*, "Integrated multi-wavelength control of an ion qubit," Nature **586**, 538–542 (2020).

[3] A. D. Ludlow, M. M. Boyd, J. Ye, E. Peik, and P. O. Schmidt, "Optical atomic clocks," Rev. Mod. Phys. **87**, 637 (2015).

[4] L. J. Mullen, A. J. C. Vieira, P. R. Herezfeld, and V. M. Contarino, "Application of RADAR technology to aerial LIDAR systems for enhancement of shallow underwater target detection," IEEE Trans. Microwave Theory Tech. **43**, 2370–2377 (1995).

[5] A. B. T. Ghisaidoobe and S. J. Chung, "Intrinsic tryptophan fluorescence in the detection and analysis of proteins: A focus on Förster resonance energy transfer techniques," Int. J. Mol. Sci. **15**, 22518–22538 (2014).

[6] D. A. Kalashnikov, A. V. Paterova, S. P. Kulik, and L. A. Krivitsky, "Infrared spectroscopy with visible light," Nat. Photonics **10**, 98–101 (2016).

[7] D. H. Card, D. L. Peterson, P. A. Matson, and J. D. Aber, "Prediction of leaf chemistry by the use of visible and near infrared reflectance spectroscopy," Remote Sens. Environ. **26**, 123–147 (1988).

[8] M. Chi, O. B. Jensen, A. K. Hansen, P. M. Petersen, and Y. Ma, "Tunable high-power external-cavity GaN diode laser systems in the visible spectral range," Laser Technol. Appl. **1**, 3 (2019).

[9] P. S. Donvalkar, A. Savchenkov, and A. Matsko, "Self-injection locked blue laser," J. Opt. **20**, 045801 (2018).

[10] D. Hofstetter, R. L. Thornton, L. T. Romano, D. P. Bour, M. Kneissl, and R. M. Donaldson, "Room-temperature pulsed operation of an electrically injected InGaN/GaN multi-quantum well distributed feedback laser," Appl. Phys. Lett. **73**, 2158–2160 (1998).

[11] S. Masui, K. Tsukayama, T. Yanamoto, T. Kozaki, S.-i. Nagahama, and T. Mukai, "CW operation of the first-order AlInGaN 405 nm distributed feedback laser diodes," Jpn. J. Appl. Phys. **45**, L1223 (2006).

[12] J. H. Kang, H. Wenzel, V. Hoffmann, E. Freier, L. Sulmoni, R.-S. Unger, S. Einfeldt, T. Wernicke, and M. Kneissl, "DFB laser diodes based on GaN using 10th order laterally coupled surface gratings," IEEE Photonics Technol. Lett. **30**, 231–234 (2017).

[13] T. J. Slight, S. Watson, S. Viola, A. Yadav, S. Stanczyk, S. Grzanka, S. Gwyn, E. Rafailov, P. Perlin, S. P. Najda *et al.*, "Recent progress in distributed feedback InGaN/GaN laser diodes," Proc. SPIE **10939**, 109390I (2019).

[14] J. A. Holguin-Lerma, M. Kong, O. Alkhazragi, X. Sun, T. K. Ng, and B. S. Ooi, "480-nm distributed-feedback InGaN laser diode for 10.5-Gbit/s visible-light communication," Opt. Lett. **45**, 742–745 (2020).

[15] A. Spott, E. J. Stanton, N. Volet, J. D. Peters, J. R. Meyer, and J. E. Bowers, "Heterogeneous integration for mid-infrared silicon photonics," IEEE J. Sel. Top. Quantum Electron. **23**, 8200810 (2017).

[16] W. Jin, Q.-F. Yang, L. Chang, B. Shen, H. Wang, M. A. Leal, L. Wu, M. Gao, A. Feshali, M. Paniccia *et al.*, "Hertz-linewidth semiconductor lasers using CMOS-ready ultra-high-*Q* microresonators," Nat. Photonics **15**, 346–353 (2021).

[17] B. Li, W. Jin, L. Wu, L. Chang, H. Wang, B. Shen, Z. Yuan, A. Feshali, M. Paniccia, K. J. Vahala *et al.*, "Reaching fiber-laser coherence in integrated photonics," Opt. Lett. **46**, 5201–5204 (2021).

[18] G. Lihachev, J. Riemensberger, W. Weng, J. Liu, H. Tian, A. Siddharth, V. Snigirev, R. N. Wang, J. He, S. A. Bhave *et al.*, "Ultralow-noise frequency-agile photonic integrated lasers," arXiv:2104.02990 (2021).

[19] R. Jones, P. Doussiere, J. B. Driscoll, W. Lin, H. Yu, Y. Akulova, T. Komljenovic, and J. E. Bowers, "Heterogeneously integrated InP\/silicon photonics: Fabricating fully functional transceivers," IEEE Nanotechnol. Mag. **13**, 17–26 (2019).

[20] J. Liu, G. Huang, R. N. Wang, J. He, A. S. Raja, T. Liu, N. J. Engelsen, and T. J. Kippenberg, "High-yield, wafer-scale fabrication of ultralow-loss, dispersion-engineered silicon nitride photonic circuits," Nat. Commun. **12**, 2236 (2021).

[21] M. Chul Shin, A. Mohanty, K. Watson, G. R. Bhatt, C. T. Phare, S. A. Miller, M. Zadka, B. S. Lee, X. Ji, I. Datta *et al.*, "Chip-scale blue light phased array," Opt. Lett. **45**, 1934–1937 (2020).

[22] T. Pan, D. Lu, H. Xin, and B. Li, "Biophotonic probes for bio-detection and imaging," Light: Sci. Appl. **10**, 124 (2021).

[23] G. Liang, H. Huang, A. Mohanty, M. C. Shin, X. Ji, M. J. Carter, S. Shrestha, M. Lipson, and N. Yu, "Robust, efficient, micrometre-scale phase modulators at visible wavelengths," Nat. Photonics **15**, 908 (2021).

[24] M. Corato-Zanarella, A. Gil-Molina, X. Ji, M. C. Shin, A. Mohanty, and M. Lipson, "Widely tunable and narrow linewidth chip-scale lasers from deep visible to near-IR," arXiv:2109.08337 (2021).

[25]E. Feltin, A. Castiglia, G. Cosendey, L. Sulmoni, J.-F. Carlin, N. Grandjean, M. Rossetti, J. Dorsaz, V. Laino, M. Duelk *et al.*, "Broadband blue superluminescent light-emitting diodes based on GaN," Appl. Phys. Lett. **95**, 081107 (2009).
[26]K. Luke, A. Dutt, C. B. Poitras, and M. Lipson, "Overcoming Si_3N_4 film stress limitations for high quality factor ring resonators," Opt. Express **21**, 22829–22833 (2013).
[27]C. Sorace-Agaskar, S. Bramhavar, D. Kharas, W. Loh, P. W. Juodawlkis, J. Chiaverini, and J. M. Sage, "Multi-layer integrated photonics from the ultraviolet to the infrared," Proc. SPIE **10510**, 105100D (2018).
[28]T. J. Morin, L. Chang, W. Jin, C. Li, J. Guo, H. Park, M. A. Tran, T. Komljenovic, and J. E. Bowers, "CMOS-foundry-based blue and violet photonics," Optica **8**, 755–756 (2021).
[29]Y. Lin, J. C. C. Mak, H. Chen, X. Mu, A. Stalmashonak, Y. Jung, X. Luo, P. G.-Q. Lo, W. D. Sacher, and J. K. S. Poon, "Low-loss broadband bi-layer edge couplers for visible light," Opt. Express **29**, 34565–34576 (2021).
[30]V. Vassiliev, V. Velichansky, P. Kersten, and F. Riehie, "Injection locking of a red extended-cavity diode laser," Electron. Lett. **33**, 1222–1223 (1997).
[31]A. S. Raja, A. S. Voloshin, H. Guo, S. E. Agafonova, J. Liu, A. S. Gorodnitskiy, M. Karpov, N. G. Pavlov, E. Lucas, R. R. Galiev *et al.*, "Electrically pumped photonic integrated soliton microcomb," Nat. Commun. **10**, 680 (2019).
[32]Y. Wang, S. Gao, K. Wang, and E. Skafidas, "Ultra-broadband and low-loss 3 dB optical power splitter based on adiabatic tapered silicon waveguides," Opt. Lett. **41**, 2053–2056 (2016).
[33]A. A. Savchenkov, S.-W. Chiow, M. Ghasemkhani, S. Williams, N. Yu, R. C. Stirbl, and A. B. Matsko, "Self-injection locking efficiency of a UV Fabry–Perot laser diode," Opt. Lett. **44**, 4175–4178 (2019).
[34]G. Stéphan, T. Tam, S. Blin, P. Besnard, and M. Têtu, "Laser line shape and spectral density of frequency noise," Phys. Rev. A **71**, 043809 (2005).
[35]P. Welch, "The use of fast Fourier transform for the estimation of power spectra: A method based on time averaging over short, modified periodograms," IEEE Trans. Audio Electroacoust. **15**, 70–73 (1967).
[36]G. Di Domenico, S. Schilt, and P. Thomann, "Simple approach to the relation between laser frequency noise and laser line shape," Appl. Opt. **49**, 4801–4807 (2010).
[37]M. H. P. Pfeiffer, J. Liu, A. S. Raja, T. Morais, B. Ghadiani, and T. J. Kippenberg, "Ultra-smooth silicon nitride waveguides based on the Damascene reflow process: Fabrication and loss origins," Optica **5**, 884–892 (2018).
[38]J. F. Bauters, M. J. R. Heck, D. D. John, J. S. Barton, C. M. Bruinink, A. Leinse, R. G. Heideman, D. J. Blumenthal, and J. E. Bowers, "Planar waveguides with less than 0.1 dB/m propagation loss fabricated with wafer bonding," Opt. Express **19**, 24090–24101 (2011).